17th World Conference on Earthquake Engineering, 17WCEE
Sendai, Japan - September 13th to 18th 2020

LATERAL RESPONSE AND CAPACITY MODELS OF CIDH PILES FOR REGIONAL SEISMIC ASSESSMENT OF CALIFORNIA BRIDGES

Y. Xie[1], Q. Zheng[2], CS W. Yang[3], J. Padgett[4], R. DesRoches[5]

[1] *Assistant Professor, Department of Civil Engineering, McGill University, Canada, tim.xie@mcgill.ca*
[2] *Ph.D. Student, School of Civil and Environmental Engineering, Georgia Institute of Technology, United States, qiu_zheng@gatech.edu*
[3] *Research Engineer II, School of Civil and Environmental Engineering, Georgia Institute of Technology, United States, cs.walter.yang@ce.gatech.edu*
[4] *Associate Professor, Department of Civil and Environmental Engineering, Rice University, United States, jamie.padgett@rice.edu*
[5] *Professor, Department of Civil and Environmental Engineering, Rice University, United States, rdr@rice.edu*

Abstract

Despite being strategically designed as elastic components, pile foundations may experience damage when subjected to strong seismic shaking and earthquake-induced soil liquefaction. Damage or failure of a pile foundation is difficult to inspect and costly to repair. Proper response and capacity models for pile foundations are required to not only quantify their damage potential but also capture their dynamic interactions with other crucial components, including columns and abutments. At the regional scale, the development of representative pile models faces the added challenge to incorporate considerable variations in pile types, soil embedment depths, soil properties, and seismic design details. As such, this paper develops probabilistic response and capacity models to facilitate the seismic assessment of California bridges region-wide. First, fiber-section based nonlinear pile models attached with *p-y* springs are built to capture different damage states of piles and realistic lateral resistances of supporting soils. Second, a large number of stochastic simulations under cyclic loading protocols are conducted for each pile type to incorporate the significant level of uncertainties stemming from soil profiles and material properties. Finally, force-displacement response results of the pile-soil systems are regressed as phenomenological hysteretic spring elements to bear the consistent backbone curves and hysteresis behaviors. Technical background, analysis frameworks, and the resultant response and capacity models are discussed based on one typical pile class, namely the cast-in-drilled-hole (CIDH) piles. An Excel workbook is also created to promote the practical use of the models. The developed multi-parameter spring models capture all essential seismic characteristics of the pile-soil systems and can be easily applied in the seismic modeling of highway bridges at large scale. Also, the suggested pile capacity models provide a sound reference to estimate the damage potential of pile foundations. Together, the proposed models are expected to significantly advance the seismic fragility, loss, and resilience assessment of regional bridge classes that are designed with various types of CIDH pile foundations.

Keywords: pile foundations; seismic response and capacity models; CIDH piles; regional-scale risk assessment

1. Introduction

Foundations are commonly designed as capacity-protected components in a bridge system [1]. Despite aims of being strategically protected, pile foundations often experience damage when subjected to strong seismic shaking and liquefaction-induced lateral spreading [2]. In this regard, proper lateral response and capacity models of pile foundations are crucial in capturing their damage potential and their dynamic interactions with other bridge components, including columns, shear keys, abutment walls, and bearings.

The seismic behavior of pile-soil systems has been investigated frequently in the literature [e.g., 3-5]. Previous studies are in general two-fold: they (1) elucidate dynamic pile-soil interaction mechanisms through simplified theoretical models; and (2) validate and develop soil resistance models to more accurately match experimental results. A distinct area of research on pile-soil behavior uses nonlinear Winkler foundation assumption to characterize soil reactions as distributed *p-y* relationships (*p* is lateral resistance, and *y* is relative displacement between the soil and pile) [e.g., 6-9]. Using *p-y* relationships, studies have provided valuable insights on the seismic behavior of pile-soil systems on a case-by-case basis.

However, achievements in these studies cannot satisfy the research needs associated with seismic risk assessment of regional bridge systems, which are designed with various types of pile foundations and are located at sites with a full spectrum of soil conditions [10]. In particular, the existing literature falls short of capturing the full-range damage states of piles, differences in design details for a mixed collection of regional pile foundations, as well as significant levels of uncertainties in soil profiles and soil material properties.

This study develops first-of-its-kind probabilistic response and capacity models of piles to facilitate regional seismic risk assessment of bridge structures. CIDH piles, a common pile type designed for California bridges statewide, are adopted as a benchmark study. A high-fidelity simulation framework is developed to incorporate a large number of heterogeneous soil profiles, nonlinear soil reactions, soil embedment effect, realistic material behaviors in piles, different design details, as well as pile-footing connection details. Cyclic pushover analyses are conducted in OpenSees on 320 pile-soil cases for each CIDH pile design. Moreover, the force-displacement response curve for each case is regressed as a response five parameter (R5P) hysteretic material to facilitate its implementation in OpenSees. Statistical distributions of R5P models are developed and verified for four CIDH pile designs embedded in five different ranges of soil depths. Finally, damage states and displacement capacity limit states are recommended to assist the seismic damage assessment of CIDH piles.

2. CIDH Piles for California Bridges

Table 1 lists seismic design details of CIDH piles that are designed in three different eras, namely Era 3 (after 1990), Era 2 (1971-1990), and Era 1 (before 1971). Despite that standard design exists (a sample design is shown in Fig. 1(a)), seismic performance of CIDH piles are expected to vary significantly due to the differences in section configuration, transverse and longitudinal reinforcements, as well as connection details between piles and footing. As will be discussed later in this study, differences in these design details not only change the lateral capacities of CIDH piles but also affect their displacement ductility. In addition, design evolution from Era 1 piles to modern piles will also alter the lateral performance of CIDH piles that have the same section diameter.

Table 1 – Seismic design details of CIDH piles

Era	Diameter (in.)	Steel Reinforcement	Confinement
Era 3	24	6 #8	#4@6.0"
	16	6 #6	W6.5@2-3"
Era 2	16	6 #5	W6.5@2-3"
Era 1	16	4 #6	#5 wire @6"

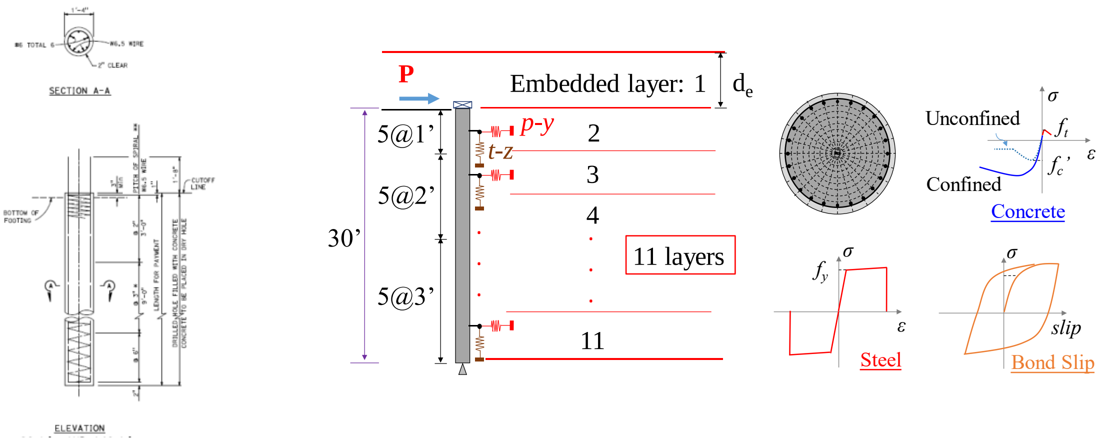

(a) Sample design (b) Numerical modeling scheme

Fig. 1 – Sample design and numerical modeling scheme of CIDH piles

3. Numerical Modeling Scheme

Finite element models were built in OpenSees [11] to simulate the lateral responses of pile-soil systems for each CIDH pile design. As shown in Fig. 1(b), the modeling scheme features a laterally-loaded pile attached by a layered soil profile. The pile was assumed to be long enough (30 ft) such that its plastic hinges can be completely developed when subjected to large lateral displacements. Force-based nonlinear column beam elements with fiber-defined sections were used to capture the full-range damage states of the pile, e.g., from concrete cracking to reinforcement fracture. 'Concrete02' material with Mander's concrete model is used to specify behaviors of concrete cover and core [12]. 'Steel02' material was applied to model the nonlinear behavior of longitudinal reinforcements [13], where a 'MinMax' material was used to simulate the fracture failure of the steel material at an ultimate strain level assumed as 20%. A zero-length section with strain penetration models for reinforcing bars [14] and zero-tensile-strength 'Concrete01' material for concrete was used to model the connection details between piles and footing.

The heterogeneous characteristic of supporting soils was captured by building 11 layers for the soil profile, where the first layer was considered to embed the pile using a random embedment depth parameter, d_e, and the remaining 10 layers were evenly distributed along with the pile depth (i.e., 3 ft for each layer in thickness). The Latin Hypercube Sampling technique has been used to generate 320 soil profiles for each pile design, incorporating uncertainties in soil properties and spatial variations in soil profiles. Table 2 lists the statistical distributions of critical parameters for soil profile sampling. First, soil type was randomly assigned between sand and clay for each layer, such that each soil profile sample may have a mixed combination of both soil types. Subsequently, the water table was randomly placed between the top of layer 2 and the bottom of layer 11 to generate a variety of saturation cases. At each layer, a normal distribution was assumed for the total unit weight of the soil, whereas uniform distributions were considered for the rest of the material parameters, defining the material behaviors of sand and clay. The ranges assigned for these material parameters were assumed to be large enough to include most of the sandy and clayey materials encountered in real bridge construction practices. Soil information from each soil profile sample was used to calculate the input parameters for *p-y* springs in OpenSees [6]. As shown in Fig. 1(b), 15 sets of nonlinear *p-y* springs were distributed with 1 ft, 2 ft, and 3 ft in spacing for the top, middle, and bottom five springs, respectively. As a result, more springs are distributed within the active length of the pile.

Table 2 – Statistical distributions of critical parameters for the soil profile sampling

Item	**Parameter**	**Lower bound**	**Higher bound**	**Distribution**	**Mean**	**Standard deviation**
Soil type	*st*	-	-	Bernoulli	Equally split[1]	
Water table	*wt*	2	11	Bernoulli	Equally split[2]	
Total unit weight	γ (pcf)	110	130	Normal	125	2.50
Sand	Φ (°)	32	42	Uniform	37	2.89
Clay	c_u (ksf)	0.5	5	Uniform	2.75	1.30
	ε_{50}	0.004	0.017	Uniform	0.011	0.0037

Note: [1] at each layer, soil type is chosen as sand or clay randomly; [2] water table is positioned randomly from the top of layer 2 to the bottom of layer 11.

3. Development of Response Five Parameter (R5P) Models for CIDH Piles

3.1 Lateral responses of pile-soil systems and R5P models

320 pushover analyses were conducted for each pile design under gradually increased displacement demands in reversed cycles. Three sample responses of the Era 3 24 in. CIDH pile are shown in Fig. 2, where the solid thin lines represent the pushover results. As is depicted, the numerical modeling scheme captures the nonlinear behavior of the CIDH pile, indicating three different response stages such as the initial elastic stage, post-yielding stage, and post-peak strength degradation stage. The solid thick lines with markers in Fig. 2 are the idealized backbone curves composed by linearly connecting three points: the yielding point (e1p, s1p), peak force point (e2p, s2p), and residual force point (e3p, s3p). To identify the yielding point, the force ratio of s1p/s2p was assumed to be 0.75.

Moreover, bridge regional seismic assessment calls for the development of simplified response models for pile-soil systems such that both their damage potential and their dynamic interactions with other bridge components can be efficiently quantified. To this end, the cyclic response of the pile-soil system was captured by a macro spring material in OpenSees using the 'Hysteretic' material command. Note that other than the backbone curve, a deformation reloading pinching factor of 0.35, a force reloading pinching factor of 0.45, and a degraded unloading stiffness power factor of 0.5 were suggested to define the 'Hysteretic' material. Fig. 2 also shows the responses provided by the 'Hysteretic' material in dashed lines, which yield consistent results against cyclic pushover outcomes.

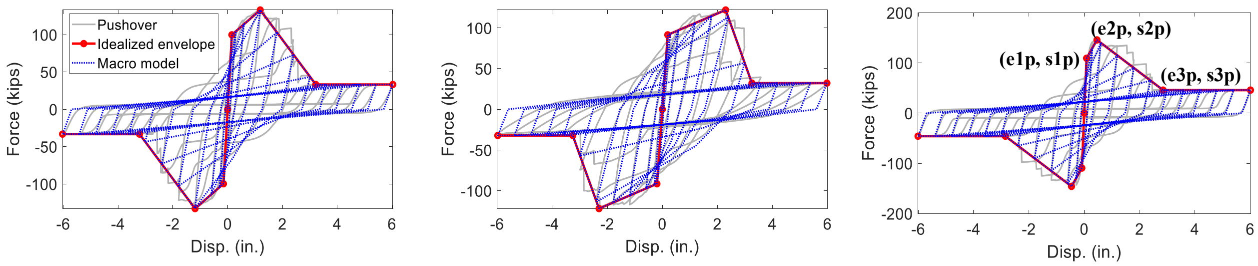

Fig. 2 – Sample responses of the Era 3 24 in. CIDH concrete pile

The five response parameters (i.e., e1p, e2p, e3p, s2p, and s3p) that define the backbone curves were transformed into ratio-based forms to facilitate model generation and implementation. As shown in Fig. 3, the parameters of e2p and s2p that define the peak force point were considered to stay in their original forms, from which three ratio-based parameters were generated, such as the residual force ratio s3p/s1p, yielding displacement ratio e1p/e2p, and ultimate displacement ratio e3p/e2p. The 320 stochastic runs provide each parameter a statistical distribution that can be further regressed as a lognormal distribution. Meanwhile, correlation coefficients among the five ratio-based parameters can be obtained from the numerical results to avoid irrational parameter combinations and unrealistic curve shapes. To this end, response models for each CIDH pile design were defined by lognormal distribution parameters (median and lognormal standard deviation) for each parameter and a correlation matrix that measures the dependency among the five parameters. Such response models are termed as the R5P models in this study.

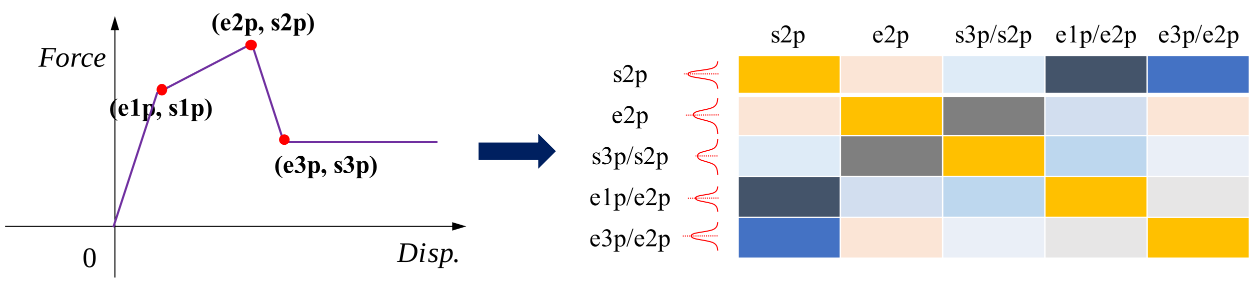

Fig. 3 – Development of R5P model for CIDH piles

3.2 R5P models for CIDH piles

As shown in Table 1 and Table 2, R5P models for CIDH piles are affected by additional factors such as soil embedment depth, section size, and design era. To save the computational cost, this study assumes that these factors are uncoupled with each other. Resultantly, the R5P models for CIDH piles consist of the base model multiplied by three factors:

$$\mathrm{R5P} = \mathrm{R5P_{base}} \cdot \delta_{eb} \cdot \delta_s \cdot \delta_{era} \tag{1}$$

where $\mathrm{R5P_{base}}$ refers to the R5P model for the base case, which was selected as the 24 in. CIDH concrete pile designed in Era 3 and embedded in a soil depth range between 2.5 ft and 7.5 ft, and δ_{eb}, δ_s, and δ_{era} are the factors that account for the influences from soil embedment, pile size, and design era, respectively.

3.2.1 R5P model for the base case

320 stochastic runs were considered for the base case to capture the uncertainties in both soil profiles and pile embedment depth, which was uniformly distributed from 2.5 ft to 7.5 ft. Fig. 4 shows the collection of samples and median backbone curves that are regressed from cyclic pushover results.

Table 3 and Table 4 summarize the proposed model for $\mathrm{R5P_{base}}$, which features a median capacity of 135 kips at a median displacement of 2.05 in. In particular, lognormal standard deviation values listed in Table 3 indicate to what extent each of the parameters would vary to incorporate uncertainties from supporting soils. Furthermore, the correlation matrix shown in Table 4 captures the dependency among the model parameters and guarantees that each correlated realization of the $\mathrm{R5P_{base}}$ model is consistent with the result from pushover analysis. Additional stochastic simulations have been carried out to determine δ_{eb}, δ_s, and δ_{era}. Because each of the numbers shown in Table 3 and Table 4 would change if a new pile design is considered, it becomes tedious and impractical to provide such matrices for each multiplier. To tackle this issue, the lognormal standard deviations in Table 3 and the correlation coefficients in Table 4 were determined by taking into account all cases for CIDH piles. In particular, each of the standard deviation values in Table 3 was chosen as the one that is close to the maximum across all cases, whereas the correlation coefficients shown in Table 4 were calculated by taking the average of all corresponding values. As a result, δ_{eb}, δ_s, and δ_{era} only alter the five median values in Table 3.

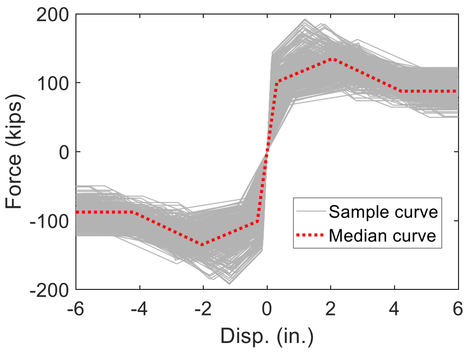

Fig. 4 – Sample and median backbone curves for the CIDH pile base case

Table 3 – Lognormal distribution parameters for $R5P_{base}$

Parameter	Median	Lognormal standard deviation
s2p (kips)	135	0.15
e2p (in.)	2.05	0.40
s3p/s2p	0.65	0.30
e1p/e2p	0.15	0.40
e3p/e2p	2.05	0.40

Table 4 – Correlation matrix for $R5P_{base}$

Parameter	s2p	e2p	s3p/s2p	e1p/e2p	e3p/e2p
s2p	1	-0.50	-0.60	0.40	0.30
e2p	-0.50	1	0.40	0.00	-0.80
s3p/s2p	-0.60	0.40	1	0.00	-0.45
e1p/e2p	0.40	0.00	0.00	1	0.00
e3p/e2p	0.30	-0.80	-0.45	0.00	1

3.2.2 Derivations of δ_{eb}, δ_s, and δ_{era}

A review of design drawing files indicates that piles can be embedded anywhere between 0 ft and 12.5 ft. Therefore, five different soil embedment ranges, namely 0 ft, 0 to 5 ft, 2.5 to 7.5 ft, 5 to 10 ft, and 7.5 to 12.5 ft, were considered to calculate δ_{eb}. Fig. 5 shows the median curves obtained by stochastic runs for ten different CIDH pile cases. As shown in the figure, stiffer and stronger lateral responses can be observed if the same pile is embedded deeper. Also, the use of a smaller diameter of 16 in. would significantly reduce the lateral capacities of CIDH piles. Results from these median curves were used to derive the closed-form expressions for the embedment multiplier δ_{eb}, and to identify values for the size multiplier δ_s. To facilitate the derivation of δ_{eb}, ranges of embedment depth were categorized and parameterized using an embedment index (*EI*) parameter, whose values are provided in Table 5.

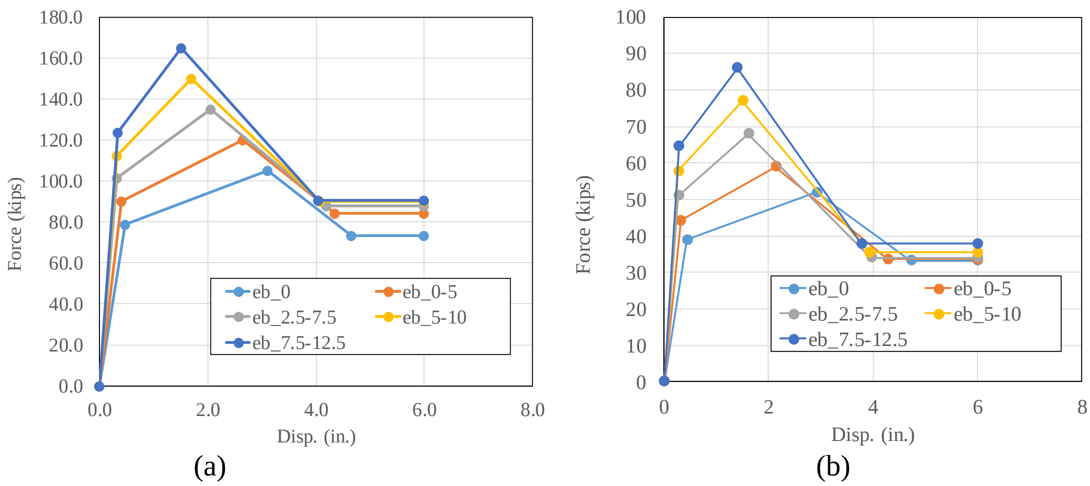

Fig. 5 – Median curves of (a) 24 in. and (b) 16 in. Era 3 CIDH piles with five different ranges of soil embedment depths

Table 5 – Embedment index (*EI*) assigned to parameterize each embedment depth range

Embedment depth	**0**	**[0, 5']**	**[2.5', 7.5']**	**[5', 10']**	**[7.5', 12.5']**
Embedment index (*EI*)	1	2	3	4	5

As shown in Eq. (1), δ_{eb}, δ_s, and δ_{era} are equal to one for the base case, yet their values would vary if a different case is of concern. The curve shapes in Fig. 5(a) and Fig. 5(b) provide a basis to calculate the embedment multiple δ_{eb}. For example, if normalizing all s2p values in Fig. 5(a) with respect to the same value for the base case, δ_{eb} for s2p can be calculated. The calculation process is illustrated in Fig. 6, where δ_{eb} for s2p and e2p are provided in Fig. 6(a), and Fig. 6(b) shows the δ_{eb} values for s3p/s2p and e3p/e2p. As can be seen from the figure, two values of δ_{eb} can be obtained at each *EI*, namely one from the 24 in. pile (Fig. 5(a)) and the other from the 16 in. pile (Fig. 5(b)). δ_{eb} were further used to develop regression curves and closed-form formulas in Fig. 6 to quantify the soil embedment effects. Note that the parameter of e1p/e2p was found to remain a constant as embedment depths change, thereby a value of one was assigned to δ_{eb} for e1p/e2p.

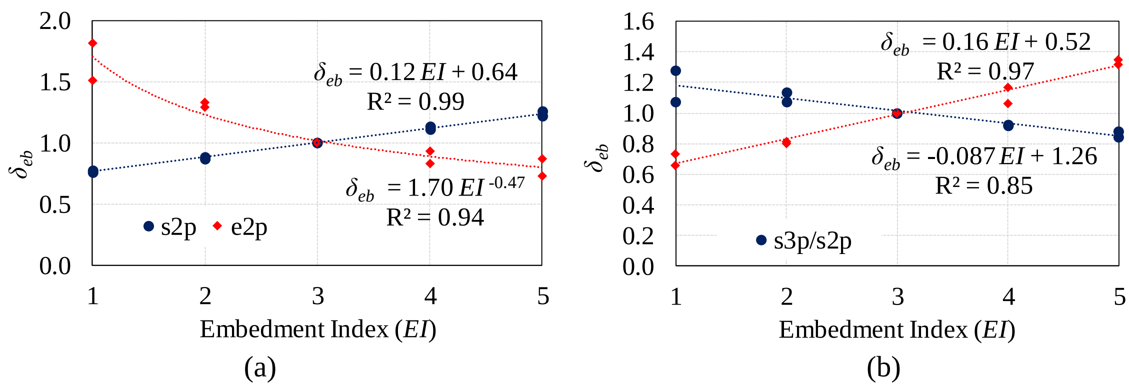

Fig. 6 – Embedment multiplier δ_{eb} for (a) s2p and e2p, and (b) s3p/s2p and e3p/e2p

Multipliers δ_s and δ_{era} are used to quantify the size and design era effects for CIDH piles, respectively. δ_s was calculated by normalizing each R5P parameter for 16 in. piles with respect to the same parameter for 24 in. piles. Two similar sets of stochastic runs have been conducted on the Era 2 and Era 1 CIDH piles, respectively, which were embedded randomly between 2.5 ft and 7.5 ft. Era multiplier δ_{era} was calculated by taking the model parameter ratios between Era 3 piles and those in the other two eras. Table 6 lists the recommended values for δ_s and δ_{era}, which are equal to one for the base case of 24 in. Era 3 piles. However, different δ_s and δ_{era} values should be applied if a different size or design Era is considered for CIDH piles. To this end, R5P models for CIDH piles are fully developed by convolving the R5P base model shown in Table 3, the soil embedment multiplier in Fig. 6, as well as the size and era multipliers in Table 6.

Table 6 – Recommended δ_s and δ_{era} values for CIDH piles

<table>
<tr><th>Multiplier</th><th>Design variation</th><th>s2p</th><th>e2p</th><th>s3p/s2p</th><th>e1p/e2p</th><th>e3p/e2p</th></tr>
<tr><td rowspan="2">δ_s</td><td>16’’</td><td>0.50</td><td>0.85</td><td>0.80</td><td>1.00</td><td>1.10</td></tr>
<tr><td>24’’</td><td colspan="5">1.00</td></tr>
<tr><td rowspan="2">δ_{era}</td><td>Era 1 & Era 2</td><td>0.88</td><td>0.75</td><td>1.00</td><td>1.12</td><td>1.35</td></tr>
<tr><td>Era 3</td><td colspan="5">1.00</td></tr>
</table>

3.3 R5P model verification

The soundness of using uncoupled multipliers to capture the lateral responses of different CIDH piles is validated by comparing R5P model results with numerical outcomes. Fig. 7 presents the comparisons of median backbone curves for three randomly selected CIDH piles that differ in pile size, design era, and soil embedment depth. As shown in Fig. 7, the dotted lines are the median backbone curves that are generated from Eq. (1), in which $R5P_{base}$ comes from the median values shown in Table 3, and the values for δ_{eb}, δ_s, and δ_{era} are given in Fig. 6 and Table 6, respectively. The solid lines in the figure are the median backbone curves obtained from the numerical analyses. The left figure in Fig. 7 verifies that δ_{eb} can yield a consistent backbone curve when the pile is embedded between 5 ft and 10 ft. The central figure examines the dependency of δ_{eb} and δ_s simultaneously, showing that the lateral performance for a smaller size (16 in.) pile embedded between 7.5 ft and 12.5 ft can be reliably predicted. Also, the last figure indicates the congruous prediction of the R5P model on the seismic performance of Era 2 16 in. piles, which attests the accuracy of using δ_s and δ_{era}. Due to limited space, other validation cases are not provided herein. However, all validation efforts generally confirm that the proposed R5P models can capture the seismic behaviors of CIDH piles.

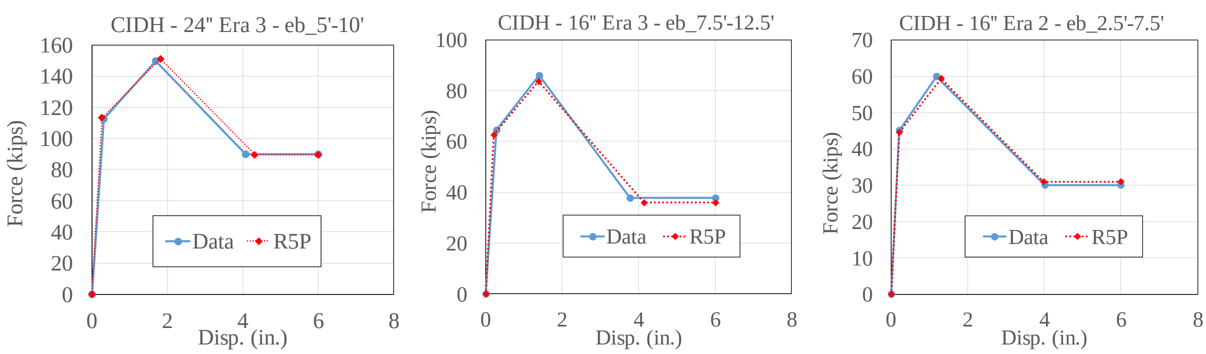

Fig. 7 – Comparisons between R5P models and numerical results for different CIDH piles

An ***Excel workbook*** has been devised to collectively present the R5P models for all CIDH pile designs shown in Table 1. The workbook features a user-interface table, the R5P model table, two figures that show the median curve and curves for 20 stochastic samples, respectively, and the R5P correlation table. To obtain

R5P models for a specific case, users only need to select soil embedment and pile design information in the user-interface table. Resultantly, data values and curves will be updated automatically in the remaining tables and figures. The ***Excel workbook*** is available from the first author upon request.

4. Capacity Limit State Models for CIDH Piles

Regional seismic assessment of bridge infrastructure convolves probabilistic seismic demand models with capacity models to develop fragility curves for crucial bridge components [10, 15]. In this regard, the development of capacity models plays a critical role in assessing the seismic damage potential of pile foundations. Pile damage states are examined herein by linking global responses (i.e., force-displacement curves) to local material performance (i.e., stress-strain behaviors) at plastic hinge locations. Fig. 8 illustrates both global and local responses of a soil-pile sample case for Era 3 16 in. CIDH piles when subjected to cyclic pushover analysis. Pile moment diagram under the peak lateral force is shown in the bottom left figure in Fig. 8, pinpointing two plastic hinge locations: the first at pile top and the second at 5 ft below the head. As is depicted in Fig. 8, when pile displacement reaches to e1p (triangle), concrete starts to crack and spall, and tensile rebar starts to yield at pile head. Also, when the pile displacement is close to e2p (circle), the concrete core at the pile head starts to crush. Simultaneously, the second plastic hinge starts to form by observing yielding reinforcing steel at 5 ft below the head. In particular, the star point in Fig. 8 corresponds to first steel fracture at pile head, resulting in considerable strength degradation in the force-displacement curve.

To this end, the linkage between fiber-scale material behavior and system-level pile performance paves the way towards a clear definition of damage states, and an objective quantification of capacity limit states for CIDH piles. As listed in Table 7, four damage states such as slight, moderate, extensive, and complete states were proposed to be consistent with those defined in previous seismic risk studies on bridges [16, 17]. Damage descriptions of these four states were considered in a way such that the same states for different bridge components would have uniform operational consequences at the bridge system level. For instance, slight damage state corresponds to mostly aesthetic damage that is observable, easily repairable, and would bear minor influence on ride experiences. However, extensive damage features significant functional loss that would call for shoring, bracing, and specific repair and retrofit measures. Under this damage state, only emergency vehicles with weight restrictions would be allowed to cross the bridge.

Accordingly, Table 7 also lists the suggested limit state models that are consistent with the damage state definition. The capacity models were developed concerning pile lateral displacements, whose values were determined by examining the relationships between global force-displacement responses and local material behaviors at plastic locations (e.g., results shown in Fig. 8). As listed in Table 7, slight damage occurs when pile displacement gets 90% of e1p; moderate damage is the state when the pile is laterally deformed to the mid-point between e1p and e2p, showing certain levels of steel yielding and/or concrete crushing. When pile displacement reaches the 20% point between e2p and e3p, extensive damage was suggested by observing significant levels of steel yielding, and the start point for rebar buckling and fracture. Last, e3p was considered as the complete damage state that corresponds to significant buckling and fracture of the steel material, pile detachment from pile cap, and significant losses of pile capacities in both lateral and axial directions. Displacement limit states were considered to possess the same lognormal distributions as those for R5P models; 0.4 was assumed as the lognormal standard deviation (i.e., β in Table 7).

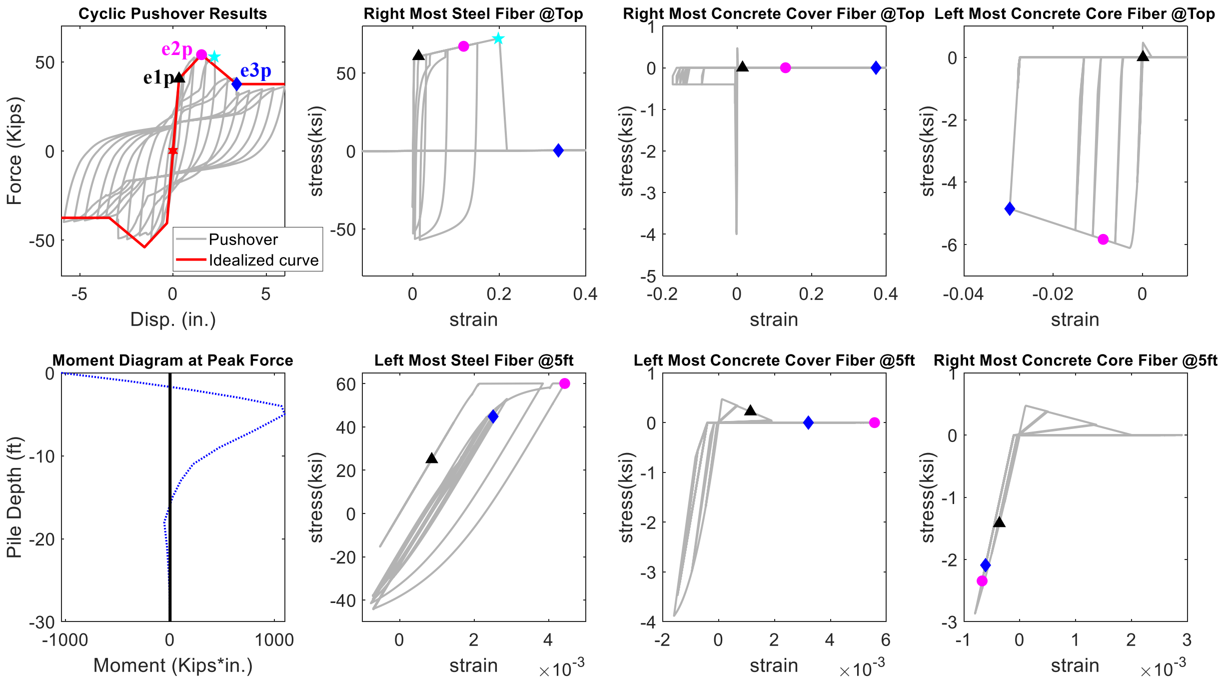

Fig. 8 – Global and local performance for a CIDH pile sample under cyclic pushover analysis

Table 7 – Damage state and capacity limit state models of CIDH piles

Capacity Model		**Slight**	**Moderate**	**Extensive**	**Complete**
Damage state		Soil-cap gap; Initial pile cracking (corrosion) at the pile head	Concrete crack and spall; rebar yield	Formation of second plastic hinge blow ground	Bucking and fracture of rebar; pile detachment from the cap; loss of lateral and axial capacities
Limit state model	Median	0.9 e1p	0.5 e1p + 0.5 e2p	0.8 e2p + 0.2 e3p	e3p
	β	0.40	0.40	0.40	0.40

5. Conclusions

This study develops lateral response and capacity models for a mixed collection of CIDH piles that are designed for California bridges statewide. Finite element models have been built for pile-soil systems to incorporate the nonlinear behaviors of soil materials, heterogeneous soil profiles, and realistic connection details between piles and footings. The full spectrum of damage scenarios of piles (i.e., from concrete cracking to steel rebar fracture) has been captured through cyclic pushover analyses. Lateral responses of pile-soil models have been regressed as a five-parameter model named as the R5P model, which consists of five sets of log-normal distribution parameters (median and standard deviation) and a correlation matrix, being able to reproduce the lateral behaviors of piles in probabilistic and realistic manners. Additional multipliers have been derived for R5P models to cover all designs of CIDH piles embedded in five different soil-depth ranges. Moreover, fiber-level material behaviors at plastic hinge locations and the corresponding global-level lateral displacement values have been utilized to define the full-range capacity models of CIDH piles.

The proposed response and capacity models can be efficiently and effectively utilized in seismic risk assessment for both individual bridges and regional bridge classes. In particular, outcomes from the current study bear tremendous benefits in (1) simulating the seismic performance of aging bridges where damage potential of CIDH piles is significant; and (2) capturing proper levels of dynamic interactions between pile foundations and other critical bridge components. Together, the proposed models for CIDH piles are able to enhance the modeling capability towards more accurate and more useful seismic fragility, loss, and resilience assessment of the bridge infrastructure in California.

6. Acknowledgements

This work has been supported by the California Department of Transportation (Caltrans) through Project P266, Task1780: Production development of generation-2 fragility models for California bridges. Any opinions, findings, and conclusions or recommendations expressed in this paper are those of the authors and do not necessarily reflect the views of the Caltrans.

7. References

[1] FHWA. (2014): *LRFD Seismic Analysis and Design of Bridges - Reference Manual*. FHWA-NHI-15-004.

[2] Nikolaou, S., Mylonakis, G., Gazetas, G., and Tazoh, T. (2001): Kinematic pile bending during earthquakes: Analysis and field measurements. *Geotechnique*, **51**(5), 425–440.

[3] Makris, N., and Gazetas, G. (1992): Dynamic pile-soil-pile interaction. Part II: Lateral and seismic response. *Earthquake Engineering & Structural Dynamics*, **21**(2), 145–162.

[4] Ashour, M., Pilling, P., and Norris, G. (2004): Lateral behavior of pile groups in layered soils. *Journal of Geotechnical and Geoenvironmental Engineering*, **130**(6), 580–592.

[5] Karatzia, X., and Mylonakis, G. (2017): Horizontal stiffness and damping of piles in inhomogeneous soil. *Journal of Geotechnical and Geoenvironmental Engineering*, **143**(4), 04016113.

[6] Boulanger, R. W., Curras, C. J., Kutter, B. L., Wilson, D. W., and Abghari, A. (1999): Seismic soil-pile-structure interaction experiments and analyses. *Journal of Geotechnical and Geoenvironmental Engineering*, **125**(9), 750-759.

[7] Curras, C. J., Boulanger, R. W., Kutter, B. L., and Wilson, D. W. (2001): Dynamic experiments and analyses of a pile-group-supported structure. *Journal of Geotechnical and Geoenvironmental Engineering*, **127**(7), 585–596.

[8] Stewart, J. P., Taciroglu, E., Wallace, J. W., Ahlberg, E. R., Lemnitzer, A., Rha, C., Khalili-Tehrani, Keowan, S., Nigbor, R. L., and Salamanca, A. (2007): Full scale cyclic large deflection testing of foundation support systems for highway bridges . Part I : Drilled Shaft Foundations. *UCLA – SGEL Report 2017/01*, UCLA Structural & Geotechnical Engineering Laboratory, USA.

[9] Khalili-Tehrani, P., Ahlberg, E. R., Rha, C., Lemnitzer, A., Stewart, J. P., Taciroglu, E., and Wallace, J. W. (2014): Nonlinear load-deflection behavior of reinforced concrete drilled piles in stiff clay. *Journal of Geotechnical and Geoenvironmental Engineering*, **140**(3), 1–14.

[10] Xie, Y., Zheng, Q., Yang, C. W., Zhang, W., Desroches, R., Padgett, J. E., and Taciroglu, E. (2019): Probabilistic models of abutment backfills for regional seismic assessment of highway bridges in California. *Engineering Structures*, 180, 452–467.

[11] McKenna, F. (2011): OpenSees: A framework for earthquake engineering simulation. *Computing in Science and Engineering*, IEEE, **13**(4), 58–66.

[12] Chang, G. A., and Mander, J. B. (1994): Seismic energy based fatigue damage analysis of bridge columns : part 1 - evaluation of seismic capacity. *National Center for Earthquake Engineering Research*, 230.

[13] Menegotto, M., and Pinto, P. E. (1973): Method of analysis for cyclically loaded R. C. plane frames including changes in geometry and non-elastic behavior of elements under combined normal force and bending. *proceedings of IABSE Symposium on Resistance and Ultimate Deformability of Structures Acted on by Well Defined Loads*, 15–22.

[14] Zhao, J., and Sritharan, S. (2007): Modeling of strain penetration effects in fiber-based analysis of reinforced concrete structures. *ACI Structural Journal*, **104**(2), 133–141.

[15] Nielson, B. G., and DesRoches, R. (2007): Seismic fragility methodology for highway bridges using a component level approach. *Earthquake Engineering & Structural Dynamics*, **36**, 823–839.

[16] FEMA. (2003). Multi-hazard loss estimation methodology earthquake model. *Hazus - MH MR4 - Technical Manual*, FEMA, Washington DC.

[17] Xie, Y., and Zhang, J. (2018): Design and optimization of seismic isolation and damping devices for highway bridges based on probabilistic repair cost ratio. *Journal of Structural Engineering*, **144**(8), 1–13.

